Theor Chem Acc (2011) 128:445–456
DOI 10.1007/s00214-010-0788-5

REGULAR ARTICLE

Causes of energy destabilization in carbon nanotubes with topological defects

Francisco J. Martín-Martínez · Santiago Melchor · José A. Dobado

Received: 13 May 2010 / Accepted: 19 July 2010 / Published online: 1 August 2010

Abstract The relative stability of a family of carbon nanotubes (CNT) with defects has been investigated theoretically with first-principles density functional theory (DFT) calculations, B3LYP/6-31G*. A set of (12,0)–(8,0) CNT heterojunctions with an increasing number ($n = 1$–4) of pentagon/heptagon defects were studied systematically in different arrangements, and the results were compared with a set of small defective graphene fragments. In addition, tubular structures with two pairs of defects distributed variedly (along and around the CNT) with increasing distances were considered. Within the defective structures, those containing the well-known Stone–Wales defect proved to be the most stable. However, when more than two pairs of defects coexisted, situations where the defects appeared together seemed to be preferred, in sharp contrast to the isolated pentagon rule (IPR) for fullerenes, although this agrees with some previous works on this topic. The junctions studied here constitute different arrangements that help us to identify which effects (geometry and energy) arise from the particular positions and orientations of the defects in nanotubes. Moreover, a close correlation was found between the energy stability and the geometric deformation, measured with the average pyramidalization angle (POAV) and the average trigonal deformation (D_{120}). For this purpose, the different contributions to molecular strain were analysed with the TubeAnalyzer software.

Published as part of the special issue celebrating theoretical and computational chemistry in Spain.

F. J. Martín-Martínez · S. Melchor · J. A. Dobado (✉)
Grupo de Modelización y Diseño Molecular,
Departamento de Química Orgánica, Facultad de Ciencias,
Universidad de Granada, 18071 Granada, Spain
e-mail: dobado@ugr.es

Keywords Carbon nanotube (CNT) · Heterojunction (HJ) · Topological defects · DFT · Stone–Wales · Sadoc knee · Dunlap knee · Isolated pentagon rule (IPR)

1 Introduction

Carbon nanotubes (CNT) [1–3] are not as perfect as they were once thought to be. This can be seen in the numerous experimental observations [4, 5] evidencing defects (either because of stress or related to their particular synthesis methods) such as vacancies, inclusions, and topological defects [6, 7] as well as dopants [8]. However, these imperfections, far from constituting a disappointment, are expected to have a significant role in the future tailoring of the electrical, chemical, and mechanical properties of these already striking structures. Hence, defects in nanotubes have attracted great attention, both theoretically [9–11] and experimentally, [12–14] because of their potential use in a great variety of applications.

A topological defect that occurs in a nanotube, not only induces a deformation in the CNT but also creates a structural alteration, which generally results in the appearance of a tube with different indices close to the defective region. The changes may cause not only a variation in the tube width but even in chirality, [15, 16] depending on the orientation of the defects. As a result, the whole structure formed by a single defect pair could be described as being composed by two different CNTs joined together and therefore are called heterojunctions (HJ) [17]. These CNT-HJs have been demonstrated to behave as diodes [18, 19], which is an evidence for their being the appropriate choice in the development of nanoelectronics [20].

Topologically, in a hexagonal graphitic network, two types of topological defects (pentagons and heptagons) may appear, each inducing disclinations of different types. While pentagons generate positive Gaussian curvature surfaces, heptagons cause negative curvature, the latter being characterized by an opposed curvature in two perpendicular directions at a certain point of the surface. In both cases, it is known that their insertion in a graphitic plane disturbs the electronic properties of the network [21]. Given the positive curvature induced by pentagons, they are widely present on any closed surface structure, like fullerenes, for which Euler's theorem states that 12 of these are needed to completely close any structure. In addition, the isolated pentagon rule (IPR) states that the most energy favoured structures (for neutral fullerenes) are those where the pentagons do not share any edge and appear maximally separated [22, 23]. Any structure with fused pentagons undergoes increased local strain and it is said to violate the IPR, although there have been reports of some IPR-violating structures [24, 25]. Given that nanotube HJs are also constituted by non-hexagonal rings, we may wonder whether CNTs also obey a similar rule.

In the case of CNTs, according also to Euler's theorem, we cannot have either one pentagon or a heptagon alone, but rather the number of pentagons and heptagons must be equilibrated, in order to retain the tubular shape of the structure. Since a pentagon and a heptagon introduce opposite 60° disclinations at the surface, their contrary effects cancel each other, leaving a single dislocation into the cylindrical shape, producing a certain geometric distortion. The amount of dislocation introduced by a heptagon–pentagon pair depends on the distance between them, as do the indices of tubes conforming the HJ. Thus, the final global deformation in the structure depends on the relative positions of the pentagon and heptagon rings in the hexagonal lattice, and therefore, defect placement is crucial as it determines both the energy stability of the structure and its structural characteristics, resulting in a global geometric deformation.

Several works have been carried out concerning the implications of different distribution of 5/7 defects along the axis and the circumference of the tube [10, 11, 26]. In their work on pairs of 5/7 defects, Charlier et al., studied the structure and electronic properties of six different HJs composed by a (12,0) CNT joined to a (11,0), (10,0), and (9,0) CNT, using one, two, and three pair of 5/7 defects, respectively. These authors compared the distribution of defects along the axis and around the circumference. In all cases, they found the HJs to be more stable when the pairs of defects are aligned along the nanotube axis rather than placed around the cylindrical circumference. Indeed, in their calculations, when two 5/7 pair defects are placed close to each other (along the circumference), those are combined to create a 5/6/7 defect (2nd order dislocation) also aligned with the axis. Furthermore, they found the average bond length in the pentagons and heptagons to be slightly longer than the one of the hexagons, and in addition, the pentagon shape is found to be planar with a very small distortion, although the heptagon is boat shaped.

In similar study, Garau et al. [11] analysed the energy characteristics of the different possible junctions between (8,0) and (6,0) CNTs using homodesmotic reactions. They characterized the four possible junctions between these two tubes using two pairs of defects (2 × 1st-order dislocation) or one 5/6/7 pair (2nd-order dislocation). Again, the 5/6/7 defect was found to be more stable than any other combination of 5/7 pair defects distributed along the circumference of the CNTs.

Both of the aforementioned studies predict that single 5/6/7 defect produces the most stable junction and, when several 5/7 pairs are needed, they prefer to appear aligned along the tube axis rather than perpendicularly.

The Stone–Wales (SW) defect can be seen as a special type of 5/7 defect [27]. SW structure is one of the most remarkable in CNTs: actually, it has been argued that around 2–5% of the carbon atoms in CNTs are involved in defective SW sites [28]. SW defects are formed by rotating a C–C bond at the hexagonal network by 90° (the so-called SW or pyracylene transformation), resulting in a twin 5/7 pair defect. It has been studied profusely [29–34], and it has been found to alter the local chemical reactivity of the nanotube [30].

The present work seeks to extend the above-mentioned studies with a systematic work including junctions concerning pairs of 5/7 defects (grouped and uniformly distributed) and SW ones. In the case of grouped defects, we compare the results with a set of small defective graphene fragments or flakes containing the same number and distribution of defects as in the respective tubular structure. The goal is to analyse a possible tendency, relating the isolated graphene flakes to the corresponding one integrated into a nanotube structure. This systematic exploration of defect positions implies the appearance of different structures, which may be qualitatively classified into two different groups, the kink-type structures, which are those where the defects are grouped on a single side of the structure, and the funnel-type ones, in which defects are uniformly spaced around the circumference, producing a smooth narrowing of the tube.

For the SW defects and related structures, we are comparing here the energy of a set of different junctions containing 2 pairs of defects in all cases. This study presents structures ranging from the most basic SW structure to that with azulene groups most separated, in a movement around and along the tube axis. In the case of the circumdating displacement, the last considered structure has

pairs of defects on opposite sites, while in the longitudinal separation the final structure has the defects at the edges of the CNT.

To gain insight into the energy differences between the different structures considered, we used our software TubeAnalyzer, so that the different geometries may be analysed visually and the resulting data from the geometries will be correlated with the energy through a parameter based on the pyramidalization and the 120° deviation angle.

2 Methodology

2.1 Computational details

The geometries and stability of the studied nanotube heterojunctions were determined within the framework of density functional theory (DFT) with NWChem 5.1. [35, 36] Becke's three-parameter functional [37] with the exchange term of Lee, Yang, and Parr [38] methodology, which was used in previous calculations on CNTs, [39] fullerenes, fragments [40] and bowl-shaped hydrocarbons [41].

All the structures were optimized at the B3LYP/6-31G* and B3LYP/3-21G* theoretical levels with and without symmetry restrictions consistently yielded the same minima.

Initial structure of the (12,0)–(8,0) HJ was generated with the CoNTub software [42, 43].

2.2 Strain quantification with TubeAnalyzer program

Every molecular structure under stress undergoes strain or deformation, which is visible as a displacement from the equilibrium geometry. In carbon nanotubes, the strain resulting from the presence of defects can be quantified through several geometrical parameters. For a planar graphene network, the equilibrium structure is characterized by the planarity of all elements and the equal 120° valence angles throughout the structure. However, if we introduce a negative disclination (removing a 60° sector, resulting in the presence of a single pentagon) in such structure, retaining its planarity, the structure is stressed and we can note that the valence angles now are not 120°. If we remove the planarity restriction, the structure combs, resulting in a conical dome, in which most of the previously distorted angles return to values near to 120°, although other kind of deformation appears, the pyramidalization. In this relaxation process, a specific kind of deformation has been substituted by other kind, so this can be seen as if the non-equilibrium between pyramidalization and 120° distortions has lead to the geometric rearrangement. Therefore, an attempt to construct a deformation parameter based on these two main components (displacement out of the plane—pyramidalization and deviation from 120° for the valence angles) will be performed here. Both pyramidalization and deviation from 120° can be evaluated on any single sp^2 carbon atom using two different geometrical parameters, the π-orbital axis vector (POAV) [44] and D_{120}, respectively.

POAV analysis [44] provides an adequate description of the geometric deformation of non-planar-conjugated organic molecules, and the current interest in fullerenes and carbon nanotubes has led to widespread application of the POAV method [45–47]. Recently, use of POAV has been questioned as it cannot be used to predict chemical reactivity [48], although POAV has been used successfully in determining the most inert fullerene [49]. In any case, we use here the POAV as a tool for measuring local strain due to presence of positive Gaussian curvature, purpose for which the POAV is the ideal parameter.

As might be inferred from the name, the method is based on vector algebra, and the only quantities necessary for this analysis are the atomic coordinates of the atoms in the molecule or fragment. The π-orbital axis vector is defined as that vector which makes equal angles to the three σ-bonds at a conjugated carbon atom, and the pyramidalization angle is determined as $\theta_P = (\theta_{\sigma\pi} - 90)°$ [50, 51].

In addition, a global deformation parameter (GDP) has been defined here for each structure as the average sum of the POAV and D_{120}. Such a global parameter characterizes the structure and provides a numerical value to represent and correlate with other numerical values such as energy.

Moreover, a complete geometrical analysis involves two additional ring-averaged parameters. First, ring bond dispersion (RBD), as a measure of the ring anisotropy, is defined as the squared mean deviation for the rings:

$$\mathrm{RBD} = \sqrt{\sum (x_i - x_a)^2} \tag{1}$$

Second, the main bond length (MBL) is defined as the mean value for all bonds composing a particular ring:

$$\mathrm{MBL} = \frac{1}{6}\sum x_i \tag{2}$$

in both cases, x_i refers to each bond in the ring.

In the present work, for a thorough investigation into bond distortions and geometrical deformations, we employ the TubeAnalyzer program [52]. This is a geometrical analysis tool for graphite structures which quickly and efficiently displays the usual distortions of graphitic structures, as well as an average value per molecule. It also provides a colour-coded representation of the geometrical parameter values to quickly detect the strain distribution within the molecule.

3 Results and discussion

3.1 Topological considerations and geometries characteristics

It has been demonstrated that two arbitrary CNTs can be joined together with only a single 5/7 defect pair [53]. Such nanotube heterojunctions can be constructed automatically with the CoNTub software [42], but the current (v1.0) version is restricted to junctions formed with a single pair of defects (pentagon/heptagon). This is because, if the tube contains two or more pairs of defects, the geometric possibilities that lead to such heterojunction are infinite. Each of these possibilities takes a different shape, depending on the particular defect location, but still is able to join the intended tubes of fixed indices. Therefore, given the huge variety of possible structures that emerge for any particular combination of interconnected indices, the present study explores the energy of different defect distributions, trying to determine the possible trends that may appear. For this, we have selected several ad hoc representative sets of HJs with a number of defects ranging from 1 to 4, connecting two CNTs of fixed values, the (12,0) and the (8,0). The selected HJs provide an overall representation of the different junctions allowed between these two specific tubes, although the mathematical possibilities are infinite.

The construction of the junctions was considerably facilitated by the fact that both connected tubes were of the *zig-zag* type, but with a different radius, thus being necessary to fulfil a slight and uniform narrowing. For a smooth radius reduction and given that the HJ requires a broadening of the tube that keeps the orientation of the chiral angle of the tubes, azulene-like structures oriented parallel to the structure's axis were used as dislocation source in order to introduce a (4,0) ribbon, a task that can be accomplished in several ways. Had the junction been composed by two chiral tubes, the operations requested would not have been so straightforward.

The azulene moiety is formed by a fused pentagon and a heptagon, but when inserted into a graphite sheet (as a 5/7 defect pair), they induce a crystalline dislocation. Such a dislocation, (see Fig. 1a) when applied parallel to the tube axis, results in the insertion of one atom row in the structure, increasing the first index of the tube by a single unit. Since it adds just one atom row, we consider the azulene group as the source of a basic first-order dislocation. Furthermore, if we separate the pentagon and heptagon through an additional hexagonal ring (namely a 5/6/7 defect), we are introducing an additional row, constituting a second-order dislocation. This is easily extended to the introduction of n hexagons between the pentagon and the heptagon in the 5/7 defect, increasing the order of the dislocation to $n + 1$ units and yielding an index increase from $(i,0)$ to $(i + n + 1,0)$ (See Fig. 1b).

However, there are many ways to achieve an nth-order dislocation. One is by introducing a single 5/6/7 defect with $n - 1$ hexagons in between, but other possibilities arise from combining multiple 5/7 defects at different positions, as shown below.

In any event, the dislocation either reduces the diameter or changes the chirality, depending on its orientation in the nanotube hexagonal network. In our particular case, azulene units appear inside a *zig-zag* CNT parallel to the tube axis, implying for each one a reduction or increase in the CNT diameter. This results in an index change from $(n, 0)$ to $(n - 1, 0)$, with the tubes remaining joined always as *zig-zag*. Therefore, it should be clear that every introduction of an azulene fragment results (if properly aligned) in a decrease/increase in only the first index of the *zig-zag* nanotube. This opens the possibility of introducing several

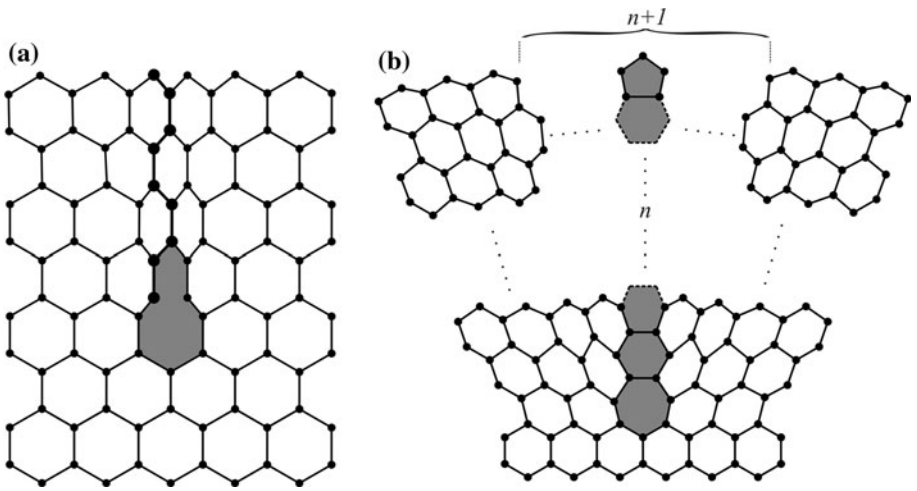

Fig. 1 **a** First-order dislocation produced by an azulene moiety (*shadowed*) in a graphene sheet. Atoms inserted by the dislocation are *highlighted*. **b** nth-order dislocation produced by azulene-like defects in a graphene sheet. n rows of hexagons are introduced in the network as consequence of $n - 1$ hexagons in the strip between pentagon and heptagon ($5/n - 1/7$ defect)

azulene units together to produce the same transition as that produced by an *n*th-order generalized azulene moiety.

Although within the different possible shapes for the HJs, Dunlap knees are the easiest to construct (and therefore, the best known), here we discuss the opposed junctions, those having the heptagon and the pentagon in the same side of the tubular structure. These can be seen as minimum-angle junctions and are also referred to as Sadoc junctions, which have the pentagon and the heptagon aligned, forming a proper disclination. This will be analysed together with different combinations of lower-order azulene moieties, so that structures can be grouped accordingly to the number, position, and magnitude of azulene moieties employed.

Here, we discuss here about the tubular structures (denoted with a T letter) formed by a certain number of azulene pentagon–heptagon pairs, from 1 to 4. If all defects are grouped (G series) in the same side of the tubular junction, these will be the T1G, T2G, T3G, and T4G structures. However, if the defects are uniformly (U series) distributed around the section of the junction, we will have T1U, T2U, T3U, and T4U structures. Note that, given a single pentagon–heptagon defect which cannot be grouped or uniformly distributed, T1G and T1U are the same structure, although either name will be used depending on the particular comparison, for the sake of consistency. Grouped structures, because of their similarity to the shape of Sadoc's junctions (reduction in the diameter only observable in a single side of the junction), can be considered as generalized Sadoc ones and may be briefly referred as Sadoc knees. On the other hand, the uniformly distributed structures have a diameter reduction in all areas around the junction, and therefore these, because of the uniform narrowing of the tube, adopt also a shape with almost 0° bending angle (this depends on the symmetry of the defect distribution), with a funnel-like shape, and therefore may be called funnel junctions.

3.2 Relative energies and geometrical deformation parameters

To gain insight into the causes of energy destabilization that derive from the number and position of topological defects, we made two separate studies of defective structures. For this, structures that were relaxed at B3LYP/3-21G* level were analysed geometrically, following two different approaches. The first consisted of varying the number of defect pairs employed in the construction of different (12,0)−(8,0) HJs. The second approach explores the variation in stability of simpler tubular structure, constructed with the help of two azulene defects, studying the effect of locating the azulene units at different distances and orientations.

3.2.1 Exploration of various (12,0):(8,0) junctions

Because of the elevated number of available structures, it was possible to construct (12,0):(8,0) structures with 1, 2, 3, and 4 pairs of 5/7 defects, while preserving the same molecular formula, ($C_{320}H_{20}$). This considerably eases the energy comparison between them, thereby providing a perfect set to explore the energy dependence of these tubular structures with the number of defects. A reasonable energy reference for all of these junctions can be found in a (10,0) CNT of selected length, which also shares the same molecular formula. This structure averages the radii and lengths of the (8,0) and (12,0) nanotubes, so that it may serve as a reference point of similar Gaussian curvature. In all cases, the comparison between these isomeric structures is straightforward. In order to compare the effects of different number and position of the pentagon–heptagon pair defects, two sets of structures were constructed: the first features all the defects on the same side of the tube, with an increasing number of pair defects up to 4, (T1G, T2G, T3G, T4G structures, where G stands for 'grouped'), while the other set presents the defect pairs distributed evenly in a circumference around the HJ, also with up to 4 defect pairs (T1U, T2U, T3U, T4U, where U stands for 'uniform' distribution). It should be noted again that T1G and T1U are the same structure, because a single defect pair cannot be uniformly distributed.

Table 1 lists the energy levels for T1G-T4G, T1U-T4U, and F1–F4, as well as the corresponding average values of four geometrical parameters, calculated with TubeAnalyzer software. These are the POAV, D_{120}, ring bond dispersion (RBD), and main bond length (MBL), which have proved to be valuable in analysing the geometric features present in CNTs [39].

Table 1 Relative energies and average geometrical values calculated with TubeAnalyzer software for T1G–T4G, T1U–T4U, and F1–F4

	E (kcal/mol)	POAV	D_{120}	RBD	MBL
T1G	102.0	95.3	2.69	0.007	1.429
T2G	151.1	95.3	2.88	0.008	1.429
T3G	182.8	95.3	3.21	0.008	1.429
T4G	183.2	95.3	3.34	0.008	1.429
T1U	102.0	95.3	2.69	0.007	1.429
T2U	152.3	95.3	2.97	0.008	1.429
T3U	164.1	95.3	3.10	0.008	1.429
T4U	193.8	95.3	3.33	0.008	1.429
F1	135.5	92.2	4.18	0.017	1.424
F2	278.6	92.3	5.39	0.022	1.426
F3	209.3	92.2	7.55	0.022	1.425
F4	196.1	90.7	9.57	0.025	1.426

As reflected in the Table 1. as well as in Fig. 8. both grouped and uniform tubular structures raise their energy level with respect to the isomeric (10,0) structure, up to about 200 kcal/mol. After the first insertion of a pentagon–heptagon defect, the structure undergoes the most noticeable change, with an increase of about 100 kcal/mol. After more defect pairs are introduced, the destabilization rises less sharply, but steadily. No dramatic energy differences can be appreciated within the two series. However, a slight feature can be noticed for structures with more than three defect pairs. For three and four defect pairs, an opposed trend appears. It may seem that three defect pairs prefer to appear uniformly distributed, while four pairs prefer to appear grouped. However, the trend marked by T4G/T4U has to be questioned, because these (12,0):(8,0) structures have almost no space for more defect pairs, and in both cases, the four defects appear at similar distances between themselves being the defects separated by only a single-ring width spacing, in both cases. So, a slight tendency for defects to prefer to be arranged most separately could be inferred from T3G/T3U, although we have to stress that this is a very minor effect.

It is also noticeable how the structures with four defect pairs have energetic values similar to the structures with three defects. We believe this is so because the additional strain introduced by more valence angles distinct from 120° is compensated by the reduction in curvature in the structure, being the T4G and T4U structures smoother in form.

With regard to the geometric values presented in Table 1, those related to bond alternation in rings (RBD and MBL) are very similar in most of the cases, while those regarding the deformation and curvature of the surface (D_{120} and POAV) are more diverse. For the later parameters, we will discuss below how these are related closely to the energy values.

In both series, the most basic (12,0):(8,0) HJ, built with just one pair of defects, proved to be the most stable one among those analysed, and its main geometric characteristics bear mentioning, in particular, the location of the most curved areas. For this, we inspected mainly the pyramidalization value for each atom, POAV, colour-coded in Fig. 2. For a better viewing, POAV values below a cut-off value of 95° have been hidden (Grey colour). Beyond the evidently curved area around the pentagon, we also notice that the narrower (8,0) tube appears more curved than the (12,0), due to its smaller radius. Additionally, what attracts our attention is the area located opposite the pentagon. Being located far from any non-hexagonal ring and where the curvature radius is similar to that for the (12,0) tube, the deformation in this region is greater. On the other hand, there are areas (see Fig. 2a, bottom) with lower POAV, in such a way that, around the HJ, we alternatively cross high and low pyramidalization zones. This, together with a noticeable line of atoms with higher pyramidalization (transversal line marked in green in tube (8,0) originating from the pentagon), results in an overall deformation of all the structure, as if the HJ would have been squeezed from the sides (that show greater planarity).

With regard to D_{120} values, considering that this parameter measures the deviation from 120° for valence angles at each atom, the most pronounced values can be found on the atoms belonging to each defect. However, it is also noticed how relatively high D_{120} values can be found in the (8,0) tube (see Fig. 2b, green atoms next to the heptagon). This reveals a deformation for the (8,0) tube, not resulting in an excess of curvature (POAV values are within a correct range), but a deformation that may be associated with an elongation of the (8,0) tube.

MBL and RBD plot (Fig. 2c,d) show high bond dispersion around both pentagon and heptagon, which could be a source of bond alternation patterns, in a behaviour similar to that near the nanotube edges, as discussed in our previous results [39]. However, periodic patterns cannot be observed here. Instead, the defect presence caused the appearance of enlarged rings (blue rings in Fig. 2d) at both sides of the pentagon and beyond the heptagon, in the (8,0) tube. This latter area corresponds to the higher D_{120} area, and thus, they may have the same origin. At the same time, from RBD, in Fig. 2c, we can see that the rings with the highest dispersion are those near the defects, as these are known to originate the appearance of bonds with an enhanced double-bond character. An additional noteworthy feature is the appearance of a ring with almost zero RBD (marked in red), between the pentagon and the border, which, considering the relatively low MBL and low POAV for the atoms belonging to that ring, we may affirm that special conditions (particular distance from the border and to the pentagon) have caused the localization of certain Clar-sextet characteristics there. That ring, distinctly marked by this exceptional low RBD, will surely have a different chemical reactivity from that of its surroundings.

Returning to the energy comparison between grouped and uniform defects in HJs, we could have the impression that the increased destabilization, for both uniform and grouped types, is a result of the also increased number of defects. However, a closer look at the defect-grouped structures (and others derived from these) will reveal that these are not actually the origin of the destabilization.

For the ‘G’ set, it becomes evident that all of these structures have two portions, the uniformly hexagonal one and the opposite side, which contains all the defects and also shows a highly curvature surface. This prompts the question concerning whether the closure of the tubular structures has a specific role or whether it merely constitutes a smooth transition, without any energy cost. To

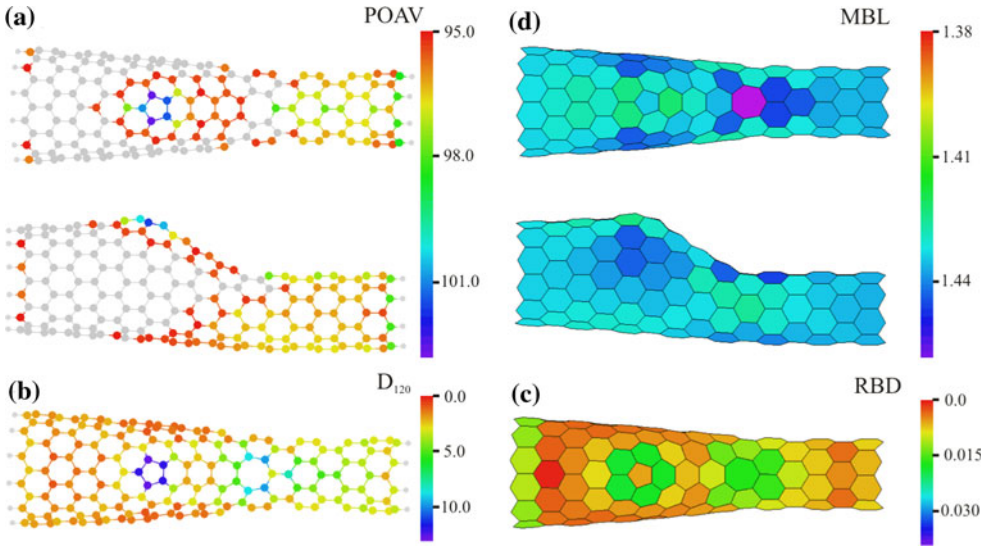

Fig. 2 POAV, D_{120}, RBD, and MBL for the T1G/T1U structure. Generated with TubeAnalyzer software

check this, we constructed non-tubular structures based on one of each T1G–T4G, which consists of flake-shaped graphitic structures that contain exactly the same defect distribution, plus a surrounding border composed of a single row of hexagons, called F1, F2, F3, F4, respectively (see Fig. 3). These also share the same stoichiometry ($C_{72}H_{22}$). Because of their reduced size, F1–F4 were fully optimized at a higher computational level (B3LYP/6-31G*). As happened to the tubular structures, the energy values for the flakes were referenced to a portion of graphene with the same molecular formula, yielding the relative energy values shown in Table 1.

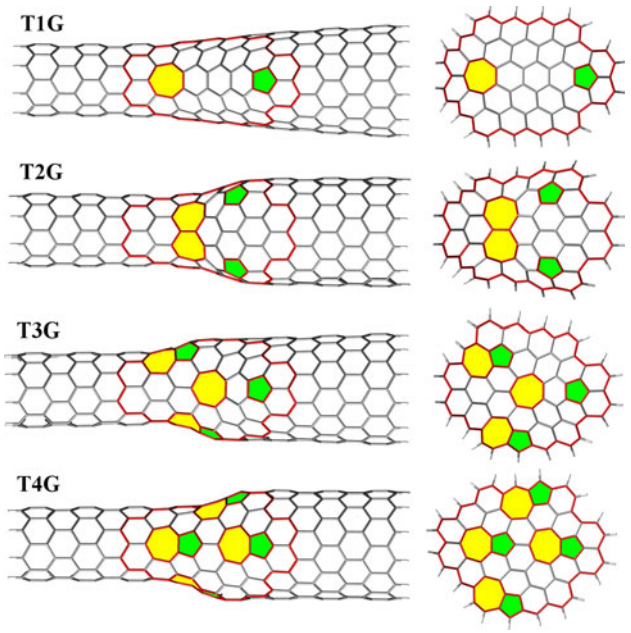

Fig. 3 (12,0):(8,0) optimized geometries calculated at B3lYP/3-21G* with formula $C_{320}H_{20}$, together with related graphene flakes containing the same distribution of defects F1–F4

Figure 3 displays the optimized geometries for (12,0)–(8,0) HJs T1G–T4G, where the contour of the derived defective graphene sheets is marked in red, next to the corresponding F1–F4. From their energy values, it is surprising to note that, after F2, the increase in defects stabilizes them instead of destabilizing them, as might be expected from the HJ energy comparison. Therefore, the mere presence of a higher number of defects does not necessarily imply the destabilization of the structure. Consequently, we needed to find where the cause of destabilization is located in flakes and also in HJs. In flakes, if more than two pairs of defects coexist, the situation where the defects appear together is preferred, in sharp contrast to the isolated pentagon rule (IPR) for fullerenes, but in agreement with previous works already discussed.

Figure 4 represents the flakes F1–F4 again, in both azimutal and lateral views, together with a bar representation of their energy values. A clear correlation appears between the deformation of the flake and the energy destabilization. From F2 to F4, as the number of defects increase, the curvature does not increase, but rather diminishes, having a less pronounced profile. A quantification of this correlation will be presented and discussed below. Bearing in mind that such a correlation exists, an explanation can be found for the slight energy differences between T3G and T3U, although we should repeat that the dependence with the inter-defect distance is very subtle, if not elusive. After correlating deformation with the energy of the grouped and uniform series, we may verify that T3U has a higher deformation than T3G, while T3U is lower in energy than T3G. Therefore, if overall energy destabilization is related to the degree of deformation, the lower energy of T3U, even after having a higher deformation, indicates that uniform distribution is favoured over the grouped ones.

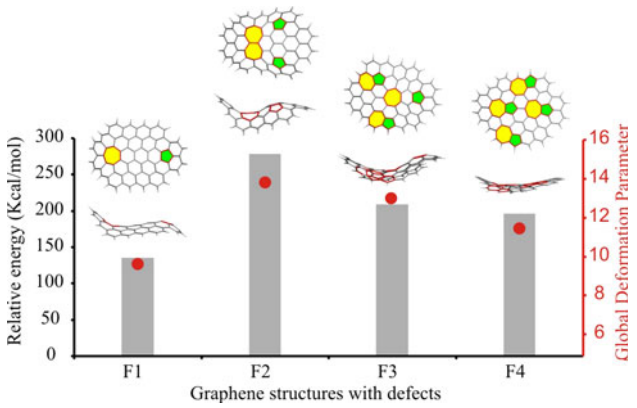

Fig. 4 Relative energy stability for graphene sheets, of molecular formula $C_{72}H_{22}$, containing the same defect distribution than the heterojunctions. Energy values are relative to the non-defective graphene flake. *Red dots* and scale correspond to the energetic values derived from the GDP (see discussion about the global deformation parameter below)

3.2.2 *Effects of longitudinal and transversal separation of 5/7 defects from Stone–Wales*

The second part of this study explores Stone–Wales defects in structures related to the HJs previously studied. Thus, we compare the energy of different junctions, optimized at the B3LYP/6-31G* level, containing 2 pairs of defects in all cases, but with different separation and orientation. These structures are still junctions, although the tubes joined have the same indices (12,0):(12,0), and all of the structures have greater symmetry, so therefore these could be called homojunctions. This study, varying almost continuously the position of the defects, constitutes a perfect benchmark where the effects of azulene presence are isolated from other factors. Among the different structures considered, both 5/7 pairs are continuously separated one from each other along the axis, in the longitudinal series (T2L0, T2L1, T2L2, T2L3, T2L4 structures) and around the circumference in the transversal series (T2T0, T2T1, T2T2, T2T3, T2T4, T2T5 structures). As in the previous (12,0):(8,0) HJs, the first structure in both sets is the same (T2L0 and T2T0), the structure being where both azulene moieties appear fused as a Stone–Wales defect. The structures can be seen in Fig. 5, where the separation between pairs of defects has been represented for the sake of clarity.

Energy data for the transversal and longitudinal variants of this structure (see Table 2) is in principle in accordance with the tendency already noted for (12,0):(8,0) HJs: the defects prefer to appear as separated as possible, which reminds the IPR. This trend is more clear in the transversal structures, although compound T2T1 seems to break this trend, because this is the most stable structure. This constitutes a Stone–Wales defect, which, in essence, keeps the whole structure of the nanotube intact except a C–C bond that it is turned. The direct connection between non-hexagonal rings makes this structure not fully comparable with the other ones, as in these, the two azulene moieties are separated, having a much more extended amount of defective area. Therefore, for the transversal series, the decay of the energy values as the azulene moieties separate is smooth and constant.

The behaviour of the longitudinal series T2L0–T2L4 is less evident, although it remains consistent with the foregoing conclusions. If T2L0 is disregarded, the next three compounds have stability around a similar value, while the last one, T2L4 shows special stability. This is undoubtedly due to the presence of the non-hexagonal ring next to the border. The absence of additional rings around these avoids

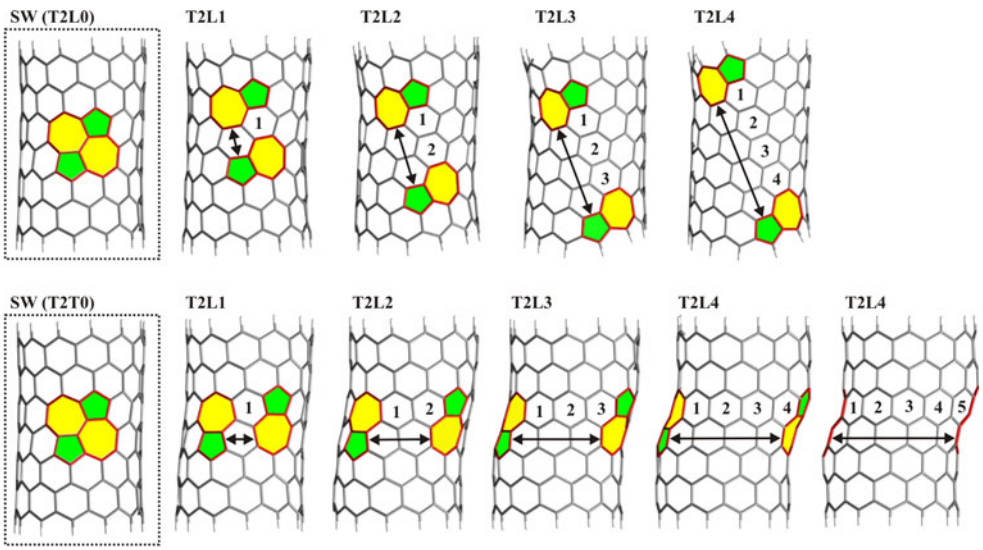

Fig. 5 B3LYP/6-31G* optimized geometries for $C_{168}H_{24}$ (**1–6**) SWCNT (12,0):(12,0) HJs composed of two pairs of defects (azulene moiety formed by a pentagon coloured in *green* and a heptagon in *yellow*) with an increasing inter-azulene distance

Table 2 Relative energy and average geometric values calculated with TubeAnalyzer software for T2T0–T2T4 and T2L0–T2L5

	E (kcal/mol)	POAV	D_{120}	RBD	MBL
T2T0	71.3	94.4	3.05	0.009	1.427
T2T1	112.5	94.4	3.14	0.010	1.427
T2T2	106.5	94.4	3.13	0.010	1.427
T2T3	102.1	94.5	3.07	0.010	1.427
T2T4	102.6	94.5	3.04	0.010	1.427
T2T5	104.2	94.4	3.05	0.010	1.427
T2L0	71.3	94.4	3.05	0.009	1.427
T2L1	111.3	94.4	3.29	0.011	1.427
T2L2	116.9	94.5	3.45	0.010	1.427
T2L3	111.6		3.64	0.010	1.427
T2L4	64.9	94.5	3.34	0.008	1.427

the excess of strain that would arise otherwise. When defects are on the border, as in the T2L4 structure, the distinct topology of the edge enables the geometry to relax.

Finally, we may compare the geometries of T2L2 and T2L4 through the representation of RBD. Average values for MBL, POAV, and D_{120} are shown in Table 2, with T2L4 having values lower than T2L2, especially in D_{120} and POAV. This accounts for the strain release in T2L4 that arises from the non-hexagonal rings in the border.

Figure 6 represents the RBD plot of T2L2 and T2L4 structures on both sides. The non-defective side of the tube is coloured in reddish values in both structures, as occur in straight, uniform nanotubes. In the defected side of the tube, this uniformity disappears, upset by the presence of the defects, which cause a higher dispersion of bonds (green rings). The distance between defects plays a role in the red uniform belt around the structure. When defects are closer, as in T2L2, it could be enough to break the red belt. However, in T2L4, the distance between pair of defects is enough to let the inter-defect area retain low RBD values, close to zero.

3.3 Correlation between the total energy and the surface deformation

Although a clear correlation has been demonstrated between the energy stability of both flakes and tubular HJ's, we need to explain this behaviour, and because of that, we will try to find a correlation between the energetic destabilization and the surface deformation. To do so, we developed a strategy based on two deformation parameters mainly related to the curvature and distortion of the surface, which are the POAV and D_{120}. RBD and MBL distortions are more related to electronic issues and therefore are not included in the parameter. The goal is to provide a single numerical value, which could have any correlation

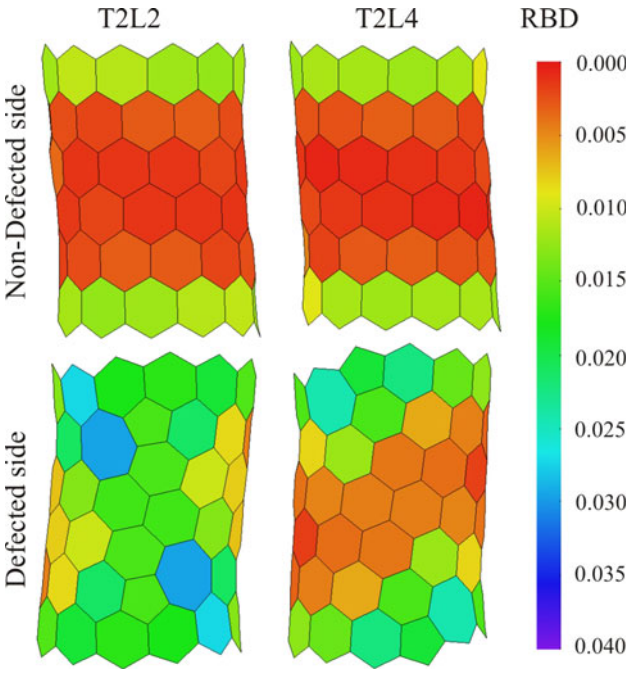

Fig. 6 RBD representation of T2L2 and T2L4 structures. Defective and non-defective sides are depicted in order to analyse the geometric uniformity break cause by the coupled defects (T2L2) in comparison with T2L4, where defects are in the border

with the total energy of the system. We refer to this as the global deformation parameter (GDP), which in a preliminary approach can be defined as a linear combination of POAV and D_{120}. However, for a good adjustment with the energy, the relative weight of each component has to be adjusted. We can find this adjustment by optimizing the correlation with the total energy. We have to clarify that this adjustment is not intended towards the obtention of a universal relationship for any graphene-based compound. This is so, because the systems studied present different chemical formula, and therefore, the destabilization values obtained relatively to a particular reference system cannot be related to averaged values of POAV and D_{120}, except if the correlated compounds belong to a set sharing the reference system, topology, and shape.

Hence, to find the correlation, following the definition in Eq. 1, we calculated the GDP as a function of a single parameter, the ratio a:b, For each a/b value chosen, a different GDP is defined, and therefore, a different correlation with the energy is found. Prior to the construction of the GDP, the a:b ratio is unknown, we have only energetic destabilization values for each set. In order to obtain the adequate ratio, we constructed a parametrized GDP as a function of the a:b ratio, and this ratio is varied and examined the resulting correlation. The optimal correlation was obtained by computing the corresponding r^2 of a linear fitting of the destabilization values and getting the maximal

r^2 value. This way the distinct proportions (for each family of compounds) of POAV and D_{120} can be found for a particular series of compounds. If (r^2) gets closer to one afterwards, this would indicate that the correlation is nearly correct.

$$\mathrm{GDP} = a \cdot \mathrm{POAV} + b \cdot D_{120} = b \cdot \left(\frac{a}{b} \cdot \mathrm{POAV} + D_{120}\right) \tag{3}$$

This procedure has been repeated in all cases, plotting several curves depending on the a:b ratio, as presented in Fig. 7. For the family of (12,0):(8,0) HJs, the relation between POAV and D_{120} is 5:1, while in the case of (12,0):(12,0) HJ's, the relation is 8:1 and 15:1 for the longitudinal and transversal sets, respectively. Even for graphene curved flakes (F1–F4), the methodology yields a correlation between deformation and destabilization, even despite the very varied forms they present and that there is no visible correlation of the energetic destabilization with POAV or D_{120} individually. However, combining both parameters, a correlation is clearly visible, indicating the need of exploring two distinct kinds of deformation in order to correctly measure the strain. For flakes F1–F4, the relationship obtained is about 5:2, indicating that for these planar systems, the weight of POAV and D_{120} is more equilibrated than in the tubular ones. Additionally, we have to notice that the correlation in these set of compounds smaller in size is slightly lower due to the more likely appearance of electronic localization effects, which maybe would need the insertion of other geometric parameters regarding bond strain or aromaticity effects.

In any case, these values maximize r^2 and highlight how for each geometry the weight of surface curvature and stretching of the surface has different contributions. Consistent with this argument, Fig. 7 shows that for (12,0):(8,0) HJs, a correct ratio is easy to find, since the curve shows a clear peak. However, in the other two cases, the curve reaches a high value in a broad range. This means that in the (12,0):(12,0) junctions, the contribution of D_{120} to the energy estimation is not significant, and consequently, the energy depends almost exclusively on the pyramidalization in the surface.

After defining the GDP and establishing the correlation procedure, we analysed in detail the different sets of structures. Before discussing particularities, it is worth stating that a very good correlation is invariably found for all the sets of structures, with r^2 values consistently over 0.9, stressing the tight correlation between the energy of the systems studied and the overall curvature of the surface.

In the case of the (12,0):(8,0) HJs, although the situation depicted in Fig. 8 could be expected (an increment on the number of defects raises the energy), this is not related with the number of defects, but with the increment in curvature. Figure 8 shows that the GDP calculated with the POAV and D_{120} (red dots) almost reproduces the energy trend. In this GDP representation, the red crosses refer to the group-defective structures, while the solid dots refer to the uniform-distributed ones. The correlation presented here leads us to conclude that geometric deformation is the main cause of the energy destabilization in these types of structures, beyond the amount of defects.

For (12,0):(12,0) HJs, the situation is similar, but in this case all junctions present two pairs of defects, although in different arrangements. The behaviour of GDP and relative energy again follow each other as we change the separation between azulene units. Thus, the different deformations, caused by a different defect arrangement, are directly connected to the energy changes in the structure.

In Fig. 9, the SW defect is revealed to be the most stable one, and correspondingly, presents the lowest deformation. However, beyond T2T2, the energy value remains almost constant (although decaying slowly), and again, the GDP reproduces the behaviour. It suggests that once the pairs of defects reach a separation in which the deformation is maximum, the strain is slowly released and, at the same time, the total energy is reduced.

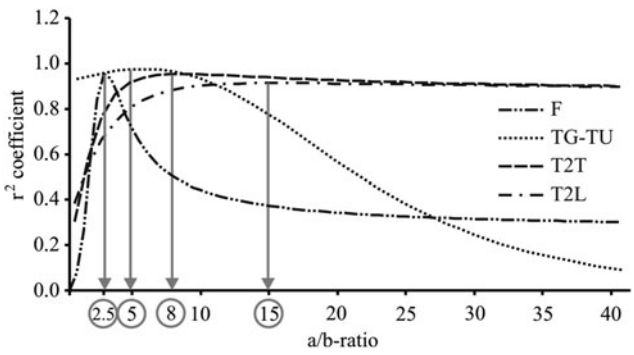

Fig. 7 Graphical representation of r^2 value against the "a:b" ratio in the determination of relative weight of each of the components in the GDP, for the different sets of molecules studied

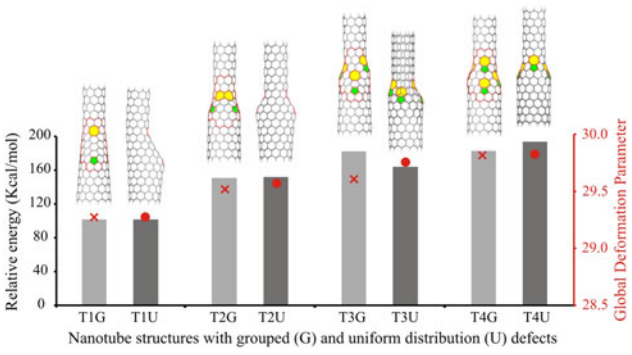

Fig. 8 Relative energy stability for (12,0)–(8,0) heterojunctions fully optimized at B3lYP/3-21G*. Energies are relative to the non-defective (10,0) CNT, with $C_{320}H_{20}$ molecular formula

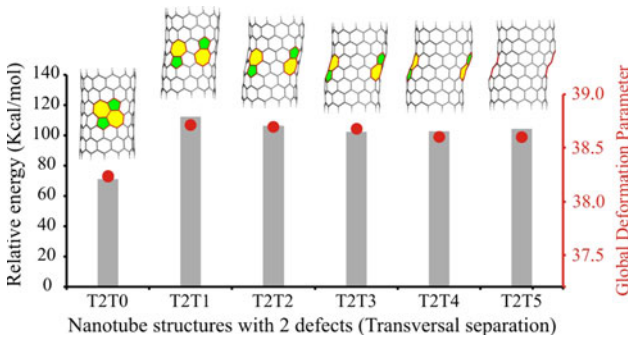

Fig. 9 B3LYP/6-31G* stability of the different heterojunctions $C_{168}H_{24}$ (T2T0–T2T5) with two pairs of defects of increasing separation, with respect to the non-defective (12,0) carbon nanotube

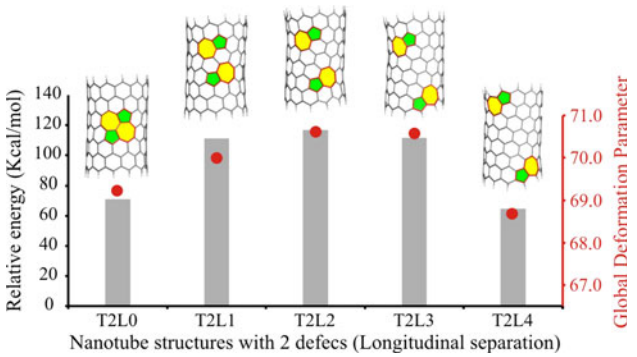

Fig. 10 B3LYP/6-31G* stability of the different heterojunctions $C_{168}H_{24}$ (T2L0–T2L5) with two pairs of defects longitudinally increasing separation, with respect to the non-defective (12,0) carbon nanotube

The situation in the case of the defects separated along the CNT is different due to the distinct arrangement at the borders (see Fig. 10). There, once more, edge effects come into play. The reasons why T2L4 is more stable than expected have been discussed above. However, it is remarkable that even in cases where the deformation and energy vary from the expected tendency (i.e. the unexpected energy stabilization due to the presence of the azulene moieties at the border), the GDP method is robust enough to relate adequately to the total energy for all of these geometries, consistently with a good correlation. The comparison between the energetical destabilization and the GDP for F1–F4 flakes can be seen in Fig. 4, where the trend is visually shown. However, although the correlations found are satisfactory, it should be noted that the proportion between POAV and D_{120} contributions is not unique but rather changes, depending on the family of compounds it is applied to. This is because the energy-reference system for each family taken for evaluating the deformation energy has different planarity, that is, the non-defective graphene portion is fully planar, while the fragment of (10,0) tube is not.

4 Conclusions

Direct comparisons of structures with grouped and uniformly distributed defects enabled us to determine whether defects show a preference to appear concentrated or dispersed. For the heterojunctions studied (12,0):(8,0), we found that there is a slight tendency for the azulene-like defects to appear as separate as possible, although under certain circumstances, they prefer to appear close to each other. In particular, defects appear stabilized if non-hexagonal rings appear fused or close to an open border, which again highlights the importance of edge effects in nanotubes. In the first case, the conjunction in the same place of two azulene units leads to a Stone–Wales defect, with a low degree of deformation, and in the second case, the absence of structural contour around the non-hexagonal rings relieves geometrical stress, allowing an energy stabilization. This trend agrees with the equivalent for pentagons inside a graphitic structure (IPR for fullerene structures), and the exceptions noted here to this trend are compatible with previous findings [10].

The different behaviour described for these two kinds of defects prompted some questions regarding the reasons that cause CNT shapes to preserve their uniformity and straight shape: When defects appear grouped on only one side of the tubular structure, it implies that approximately 3/4 of the molecular surface remains perfectly plain. In other words, CNTs are cylindrical molecules that try to remain so.

Furthermore, pentagons and heptagons are found to generate geometrical bond alternation patterns as edge effects do, and thus, they both can be classified, together with CNT borders, as sources of geometrical disturbances. The coupling of these disturbance sources with others, such as open borders, may cause geometrical features with consequences in the chemical reactivity of individual portions of the structure. Borders themselves are found to relax strain when defects are located in them, considerably decreasing the energy.

All these considerations are based on both energy parameters and geometric ones, which are found to be strongly connected. Indeed, a close correlation between the relative energy for each compound (referenced to a non-defective structure) and its geometrical deformation (quantified in a global deformation parameter constructed through local parameters such as POAV and D_{120}) is found in all cases. This correlation suggests a possible general mathematical relation between deformation and energy destabilization, valid for smooth curvature changes in general graphitic systems.

Acknowledgments This work has been financed by the "Consejería de Innovación Ciencia y Empresa-Junta de Andalucía" (ref. FQM-840).

FJMM and SM also acknowledged "Consejería de Innovación Ciencia y Empresa-Junta de Andalucía" (ref. FQM-840) and the "Ministerio de Educación" (CTQ2007-65112) for their contracts. We also thank the ""Centro de Servicios de Informática y Redes de Comunicaciones""(CSIRC), University of Granada, for providing the use of its computing facilities (UGRGRID). Mr. David Nesbitt revised the English manuscript.

References

1. Iijima S (1991) Nature 354:56
2. Iijima S, Ichihashi T (1993) Nature 363:603
3. Dresselhaus MS, Dresselhauss G, Eklund RC (1996) Science of fullerenes and carbon nanotubes. Academic Press, San Diego
4. Ebbesen TW, Takada T (1995) Carbon 33 7:973
5. Kosaka M, Ebbesen TW, Hiura H, Tanigaki K (1995) Chem Phys Lett 233:47
6. Iijima S, Ajayan PM, Ichihashi T (1992) Phys Rev Lett 69:3100
7. Iijima S, Ichihashi T, Ando Y (1992) Nature 356:776
8. Charlier J-C (2002) Acc Chem Res 35:1063
9. Meunier V, Lambin Ph (1998) Phys Rev Lett 81:5588
10. Charlier J-C, Ebbesen TW, Lambin Ph (1996) Phys Rev B 53:11108
11. Garau C, Frontera A, Quiñonero D, Costa A, Ballester P, Deyá PM (2004) Chem Phys 303:265
12. Yao Z, Postma HWC, Balents L, Dekker C (1999) Nature 402:273
13. Hashimoto A, Suenaga K, Gloter A, Urita K, Iijima S (2004) Nature 430:870
14. Ouyang M, Huang JL, Cheung CL, Lieber CM (2001) Science 291:97
15. Dunlap BI (1992) Phys Rev B 46:1933
16. Dunlap BI (1994) Phys Rev B 49:5643
17. Wei D, Liu Y (2008) Adv Mater 20:2815
18. Chico L, Benedict LX, Louie SG, Cohen ML (1996) Phys Rev B 54:2600
19. Collins PG, Zettl A, Bando H, Thess A, Smalley RE (1997) Science 278:100
20. Xu H (2005) Nat Mat 4:649–650
21. Tamura R, Tsukada M (1994) Phys Rev B 49:7697
22. Austin SJ, Fowler PW, Manolopoulos DE, Orlandi G, Zerbetto F (1995) J Phys Chem 99:8076
23. Austin SJ, Fowler PW, Orlandi G, Manolopoulos DE, Zerbetto F (1994) Chem Phys Lett 226:219
24. Yang S, Popov AA, Dunsch L (2007) Angew Chem Int Ed Engl 46:1256
25. Ewels CP (2006) Nano Lett 6:890
26. Fa W, Yang X, Chen J, Dong J (2004) Phys Lett A 323:122
27. Stone AJ, Wales DJ (1986) Chem Phys Lett 128:501
28. Monthioux M (2002) Carbon 40:1809
29. Zhou LG, Shi San-Qiang (2003) Appl Phys Lett 83:1222
30. Lu X, Chen Z, Schleyer PvR (2005) J Am Chem Soc 127:20
31. Pan BC, Yang WS, Yang J (2000) Phys Rev B 62:12652
32. Ding F (2005) Phys Rev B 72:245409
33. Zhou T, Yang L, Wu J, Duan W, Gu BL (2005) Phys Rev B 72:193407
34. Dinadayalane TC, Leszczynski J (2007) Chem Phys Lett 434:86
35. Bylaska EJ, de Jong WA, Kowalski K, Straatsma TP, Valiev M, Wang D, Aprà E, Windus TL, Hirata S, Hackler MT, Zhao Y, Fan P-D, Harrison RJ, Dupuis M, Smith DMA, Nieplocha J, Tipparaju V, Krishnan M, Auer AA, Nooijen M, Brown E, Cisneros G, Fann GI, Früchtl H, Garza J, Hirao K, Kendall R, Nichols JA, Tsemekhman K, Wolinski K, Anchell J, Bernholdt D, Borowski P, Clark T, Clerc D, Dachsel H, Deegan M, Dyall K, Elwood D, Glendening E, Gutowski M, Hess A, Jaffe J, Johnson B, Ju J, Kobayashi R, Kutteh R, Lin Z, Littlefield R, Long X, Meng B, Nakajima T, Niu S, Pollack L, Rosing M, Sandrone G, Stave M, Taylor H, Thomas G, van Lenthe J, Wong A, Zhang Z (2006) NWChem, a computational chemistry package for parallel computers, version 5.0. Pacific Northwest National Laboratory, Richland, Washington, DC, 99352-0999, USA
36. Kendall RA, Apra E, Bernholdt DE, Bylaska EJ, Dupuis M, Fann GI, Harrison RJ, Ju J, Nichols JA, Nieplocha J, Straatsma TP, Windus TL, Wong AT (2000) Comput Phys Commun 128:260
37. Becke ADJ (1993) Chem Phys 98:5648
38. Lee C, Yang W, Parr RG (1988) Phys Rev B 37:785
39. Martín-Martínez FJ, Melchor S, Dobado JA (2008) Org Lett 10:1991
40. Melchor S, Dobado JA, Larsson JA, Greer JC (2003) J Am Chem Soc 125:2301
41. Melchor S, Molina JM (1999) J Comput Chem 20:1412
42. Melchor S, Dobado JA (2004) J Chem Inf Comput Sci 44:1639
43. http://www.ugr.es/local/gmdm/contub.htm
44. Haddon RC (1988) Acc Chem Res 21:243
45. Haddon RC (1993) Science 261:1545
46. Chen Y, Haddon RC, Fang S, Rao AM, Eklund PC, Lee WH, Dickey EC, Grulke EA, Pendergrass JC, Chavan A, Haley BE, Smalley RE (1998) J Mater Res 13:2423
47. Srivastava D, Brenner DW, Schall JD, Ausman KD, Yu M, Ruoff RS (1999) J Phys Chem B 103:4330
48. Osuna S, Swart M, Campanera JM, Poblet JM, Solá M (2008) J Am Chem Soc 130:6206
49. Haddon RC, Scuseria GE, Smalley RE (1997) Chem Phys Lett 272:38
50. Haddon RC, Scott LT (1986) Pure Appl Chem 58:137
51. Haddon RC (1986) J Am Chem Soc 108:2837
52. TubeAnalyzer, a program written by S. Melchor, Grupo de Modelización y Diseño Molecular, Dpto. de Química Orgánica, Universidad de Granada, Spain, 2007. See ref. 39 for further details
53. Melchor S, Khokhriakov NV, Savinskii SS (1999) Mol Eng 8:315